International Journal of Thermophysics, Vol. 17, No. 1, 1996

Phase Transitions and Quantum Effects in Adsorbed Monolayers[1]

P. Nielaba[2]

Phase transitions in absorbed (two-dimensional) fluids and in absorbed layers of linear molecules are studied with a combination of path integral Monte Carlo (PIMC), Gibbs ensemble Monte Carlo (GEMC), and finite size scaling techniques. For a classical (nonadditive) hard-disk fluid the "critical" nonadditivities, where the entropy-driven phase separations set in, are presented. For a fluid with internal quantum states the gas–liquid coexistence region, tricritical, and triple points can be determined, and a comparison with density functional (DFT) results shows good agreement for the freezing densities. Linear N_2 molecules adsorbed on graphite (in the $\sqrt{3} \times \sqrt{3}$ structure) show a transition from a high-temperature phase to a low-temperature phase with *herringbone* ordering of the orientational degrees of freedom. The order of the transition is determined in the anisotropic planar–rotor model as a weak first-order transition. The effect of quantum fluctuations on the herringbone transition is quantified by PIMC and classical simulational methods. The values of the order parameter at low temperatures and the transition temperature are both lowered by roughly 10% due to quantum effects. Rounding effects of the phase transition in adsorbed layers of $(N_2)_x$ $(CO)_{1-x}$ for $x < 7\%$ are analyzed by Monte Carlo (MC) methods, and the ground state ordering for the transition in the adsorbed pure CO system is discussed, from ab initio potentials.

KEY WORDS: adsorbed layers; Gibbs ensemble Monte Carlo; path integral Monte Carlo; phase transitions.

1. INTRODUCTION

Two-dimensional (2D) layers at surfaces have become an interesting field of research during the last decade [1]. Most of the phase transitions in these systems occur at fairly low temperatures, and for many aspects of the behavior quantum effects need to be considered. This holds in particular if one is concerned with adsorbed molecules at surfaces, since the molecules

[1] Paper presented at the Twelfth Symposium on Thermophysical Properties, June 19–24, 1994, Boulder, Colorado, U.S.A.

[2] Institut für Physik, Universität Mainz, D-55099 Mainz, Germany.

0195-928X/96/0100-0157$09.50/0

have internal degrees of freedom which need to be treated quantum-mechanically even if the translational degrees of freedom can still be treated classically. Linear N_2 molecules adsorbed on graphite (in the $\sqrt{3}\times\sqrt{3}$ structure) show a transition from a high-temperature phase to a low-temperature phase with *herringbone* ordering of the orientational degrees of freedom. In Section 2, the order of the transition is determined in the anisotropic planar–rotor model by analysis of the correlation length ξ near the transition temperature T_0. The simulation data, extrapolated to T_0, yield a large but finite ξ at T_0, demonstrating that the herringbone ordering is a weak first-order transition. The effect of quantum fluctuations on the herringbone transition is quantified by PIMC and classical simulational methods. Quasiclassical and quasiharmonic calculations agree for high and low temperatures, respectively, but only PIMC gives good results over the entire temperature range. In Section 3, a study of the properties of 2D model fluids with GEMC techniques is presented. In particular, the entropy-driven phase separation in the case of a nonadditive symmetric hard-disk fluid is analyzed, and the critical line of nonadditivities as a function of the system density separating the mixing/demixing regions can be located by a combination of GEMC with finite-size scaling techniques. A comparison with a simple approximation is shown. PIMC and GEMC techniques are then combined in order to locate the gas–liquid coexistence densities for a fluid with classical degrees of freedom and internal quantum states, a comparison with NVT-ensemble results and mean field (MF) predictions is presented, and a DFT approach is outlined. In Section 4, the random field-induced rounding of the Ising-type transition in physisorbed $(CO)_{1-x}(N_2)_x$ mixtures is studied. Good qualitative agreement with recent experiments is obtained with a simple model.

2. ORIENTATIONAL PHASE TRANSITIONS IN ADSORBED MONOLAYERS

For many years adsorbed layers of N_2 on graphite have served as a prototype example to study phase transitions in 2D. The phase diagram [2] includes below 50 K a registered phase having a commensurate $(\sqrt{3}\times\sqrt{3})\,R30°$ structure. The orientations of the molecular axes undergo in this phase an *orientational* phase transition at around 27 K to the "2-in" herringbone phase, which retains the translationally ordered $\sqrt{3}$ structure of the molecular centers of mass. The herringbone phase transition has been investigated [3] by MC simulations using the anisotropic planar–rotor (APR) model. The APR Hamiltonian [5]

$$H = K(N_2) \sum_{\langle i,j \rangle}^{N} \cos[2\varphi(\mathbf{R}_i) + 2\varphi(\mathbf{R}_j) - 4\Theta_{ij}] \tag{1}$$

is used to model the quadrupolar interactions between the $N=L^2$ molecules; all angles are measured relative to one symmetry axis of the triangular lattice, and Θ_{ij} is the angle connecting lattice sites $\mathbf{R}_i$ and $\mathbf{R}_j$. The rotators $\{\varphi(\mathbf{R}_i)\}$ are pinned with their center of mass on a triangular lattice $\{\mathbf{R}_i\}$ representing the $(\sqrt{3}\times\sqrt{3})$ $R30°$ structure, and only nearest-neighbor interactions $\langle i,j\rangle$ are taken into account. The coupling constant $K(N_2)=33$ K is obtained [5] from the electrostatic quadrupole moment of N_2 and the $\sqrt{3}$-lattice constant is $a=4.26$ Å. The correlation functions are defined as $\Gamma_\alpha(l)=\langle(1/N)\sum_{i=1}^{N}\cos[2\varphi(\mathbf{R}_i)+2\varphi(\mathbf{R}_i+l\mathbf{a}_\alpha)]\rangle$ along the three symmetry axes, where $\{\mathbf{a}_\alpha\}$ denotes lattice vectors ($|\mathbf{a}_\alpha|=a$) along these axis and l runs over the neighbors along these directions. Although it is known that the decay of $\Gamma_\alpha(l)$ for large distances l should be exponential, $\Gamma_\alpha(l)\propto\exp[-l/\xi]$, an estimation of ξ from simulations is difficult. For small l there may be strong systematic corrections to this law, while for large l there are not only severe statistical problems but also systematic corrections due to the periodic boundary conditions, i.e., $\Gamma_\alpha(l)=\Gamma_\alpha(L-l)$. Thus ξ often depends on the range of l used in a fit to the exponential decay law. These problems are avoided by the procedure [6] defining ξ_l via $\delta_m \ln\Gamma_\alpha(l):=\ln[(\Gamma_\alpha(l)-\Gamma_\alpha(\infty))/(\Gamma_\alpha(l+m)-\Gamma_\alpha(\infty))]=m/\xi_l$, where $\Gamma_\alpha(\infty):=\Gamma_\alpha(L/2\gg l\gg\xi)$ denotes the constant asymptotic value of $\Gamma_\alpha(l)$ which vanishes in the disordered phase. The advantage of this approach is that no (possibly uncontrolled) fitting is involved and, especially, that the range where ξ_l approximates the true ξ can be assessed by inspection. If a plot of $\delta_m \ln\Gamma_\alpha(l)$ versus l yields a *plateau* for a certain window of distances l, then ξ may safely be extracted from such a plateau value. The linear dimensions in our simulations [3] were $L=60$, 90, 120, and 180; the statistical effort went up to 1,500,000 MC sweeps over the lattice. ξ^{-1} is plotted in Fig. 1 as a function of temperature. The behavior of ξ^{-1} demonstrates that the correlation length increases upon approaching T_0 but without showing even an onset of a divergence upon coming close to T_0; it should be noted that ξ is measured as close as 2% (0.3%) from T_0 for $T>T_0$ ($T<T_0$) (see Fig. 1) and that roughly one decade in reduced temperature is covered from both above and below. The temperature dependence of the data suggests extrapolating ξ^{-1} linearly, which yields a *finite* $\xi_+\approx 23$ ($\xi_-\approx 12$) upon approaching T_0 from above (below). Thus, judging from the behavior of ξ, one can conclude that the herringbone transition of the APR model is a weak first-order transition.

Now the problem is addressed to *quantify* the effect of *quantum fluctuation* on the orientational ordering in this molecular system. An efficient PIMC scheme [9] for rotational motion was used to study this many-body system [4]. The system consists of $N=900$ quantum N_2 rotators; the Trotter dimensions went up to $P=500$. The molecular centers of mass are

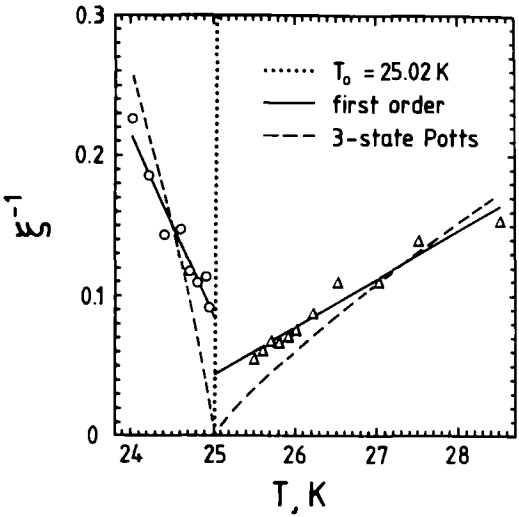

Fig. 1. Inverse effective correlation length ξ^{-1} in units of the lattice constant $a = 4.26$ Å as a function of temperature; the extrapolated transition temperature $T_0 = 25.02 \pm 0.08$ K as obtained independently from energy cumulants is marked by the dotted line. Solid lines correspond to a fit assuming a simple linear dependence $\xi = \xi_{\pm} + C_{\pm} |1 - T/T_0|$ expected near T_0 for a first-order transition, while dashed lines assume the critical behavior of the three-state 2D Potts class, $\xi = \xi_0^{\pm} |1 - T/T_0|^{-\nu}$ with [7] $\nu = 5/6$ and [8] $\xi_0^+ / \xi_0^- = 4.1$. Circles and triangles denote Monte Carlo data.

pinned on a regular trigonal $\sqrt{3}$-superlattice found experimentally [2], the interaction potentials were taken from the literature [10], and the rotational constant Θ_{N_2} was 2.9 K. The herringbone order parameter (OP) $\Phi = \langle [\sum_{\alpha=1}^{3} \Phi_\alpha^2]^{1/2} \rangle$ is defined [4] as

$$\Phi_\alpha = \frac{1}{NP} \sum_{j=1}^{N} \sum_{s=1}^{P} \sin(2\varphi_j^{(s)} - 2\eta_\alpha) \exp[i \mathbf{Q}_\alpha \mathbf{r}_j] \tag{2}$$

where $\mathbf{Q}_1 = 2\pi(0, 2/\sqrt{3})/a'$, $\mathbf{Q}_2 = 2\pi(-1, -1/\sqrt{3})/a'$, $\mathbf{Q}_3 = 2\pi(1, -1/\sqrt{3})/a'$, and $\eta_1 = 0$, $\eta_2 = 2\pi/3$, $\eta_3 = 4\pi/3$, $a' = \sqrt{3}\, a$, and $a = 2.46$ Å. The central quantity is the OP as a function of temperature; see Fig. 2. The critical temperature T_c of the classical system can be located around 38 K. At high temperatures, the quantum curve of the OP merges on the classical curve, whereas it starts to deviate below T_c. Qualitatively, quantum fluctuations lower the ordering and thus the quantum OP is always smaller than the

classical counterpart. The inclusion of quantum effects results in a nearly 10% lowering of T_c. The quantum system cannot reach the maximum herringbone ordering even at extremely low temperatures: the quantum librations depress the saturation value by 10%. In Fig. 2, the OP and total energy are compared with standard *approximate theories* valid for low and high temperatures. One can clearly see how the quasiclassical Feynman–Hibbs curve matches the "exact" quantum data above 30 K. However, just below the phase transition, this second-order approximation in the quantum fluctuations fails and yields *uncontrolled* estimates: just below the point of failure it gives classical values for the OP and the herringbone ordering even *vanishes* below 5 K. On the other hand, the quasiharmonic theory comes from the other end of the temperature axis and yields very accurate data below 5 K. The PIMC simulations, however, yield exact results over the *whole* temperature range.

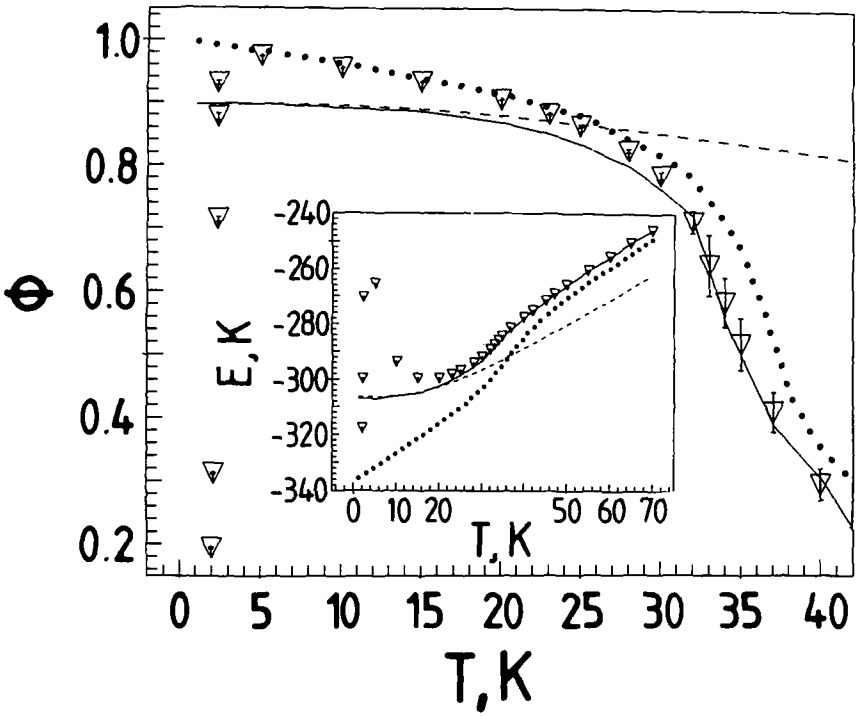

Fig. 2. Herringbone order parameter and total energy for N_2 (X_1 model with Steele's corrugation). Quantum simulation, solid line; classical simulation, dotted line; quasiharmonic theory, dashed line; Feynman–Hibbs simulation, triangles. Lines are linear connections of the data.

3. PHASE TRANSITIONS IN CLASSICAL AND QUANTUM 2D FLUIDS

Phase transitions in systems with purely repulsive interaction have received much attention recently [11]. In this section a system of hard disks (of diameter d) is considered with N_A particles of type A and N_B particles of type B and interaction potential U ($U(r_{12}) = \infty$ for $r_{12} < d_{s_1 s_1}$ and zero else, r_{12} is the distance of two particles, s_1, $s_2 \in \{A, B\}$ are their species, and $d_{AA} = d_{BB} = d$, $d_{AB} = d + \Delta/2$). The total number of particles $N = 512$ and the total volume V is fixed and thus the average density $\rho^* = \rho * d^2 = Nd^2/V$. Due to the additional repulsion between A and B-type particles, one can expect a phase separation into an A-rich and a B-rich fluid phase for large values of $\Delta > \Delta_c$ and fixed total density. Since the phase separation is driven by entropy, only a small interfacial free energy is expected in the case of phase coexistence. In order to locate the critical values Δ_c as a function of ρ^* even in such extreme situations, the GEMC simulation techniques [12] have been combined [14] with the block analysis finite-size scaling techniques [13]. Each of the 10^6 MC steps consisted of 400 attempted moves, 20 particle exchange, and 2 volume change attempts. A first approximation for the critical line l_c, defined by $\rho_c^*(\Delta_c)$, can be computed in analogy to a study in three dimensions [15] by convex envelope arguments for the free energy, resulting in the compact expression

$$\rho_c^*(\Delta_c) = \frac{4}{\pi}\left(1 - \sqrt{\frac{\Delta}{d+\Delta}}\right) \tag{3}$$

The critical points were obtained by inspection of number-difference histograms $P_L(N_A - N_B)$ on different length scales L obtained by subdivision of the simulation boxed of sizes V_1 and V_2 ($V_1 + V_2 = V$) into smaller subsystems of size $L \times L$. For $\Delta < \Delta_c$, the distributions are all singly peaked; for larger Δ a single-peak structure of $P_L(N_A - N_B)$ results for large L and a double-peak structure for small L. An analysis of these histograms with the cumulants $U_L = 1 - \langle (N_A - N_B)^4 \rangle_L / 3 \langle (N_A - N_B)^2 \rangle_L^2$ allows a determination of critical points, due to the cumulants L-invariance at the critical point. The GEMC results for points on the critical line are $(\rho_c^*, \Delta_c/d) = (0.6, 0.562 \pm 0.04)$, $(0.55, 0.66 \pm 0.01)$, $(0.5, 0.789 \pm 0.01)$, $(0.499 \pm 0.01, 0.85)$, $(0.5 \pm 0.02, 0.9)$, $(0.508 \pm 0.03, 0.95)$, $(0.46 \pm 0.02, 1)$. Similarly to the prediction of Eq. (3), ρ_c is a decreasing function of Δ_c, however, at a given density the GEMC results for Δ_c are about 20% larger than the predictions of Eq. (3).

Now the results of a novel combination of GEMC and PIMC simulation techniques [14] are presented. In particular, the gas–liquid transition of a model fluid with internal quantum states is studied. The Hamiltonian is given by

$$H = \sum_{i=1}^{N} \frac{\mathbf{p}_i^2}{2M} - \frac{\omega_0}{2} \sum_{i=1}^{N} \sigma_i^x + \sum_{i<j} U(r_{ij}) - \sum_{i<j} J(r_{ij})\, \sigma_i^z \sigma_j^z \tag{4}$$

M is the particle mass, $\mathbf{p}_i$ is the momentum of particle i, r_{ij} is the distance between particle i and particle j, and σ^x and σ^z are the usual Pauli spin-1/2 matrices. U is a hard-disk potential for particles with diameter d and $J(r) = J$ for $d < r < 1.5d$ and zero elsewhere. In the adiabatic approximation (large M), one assumes a separation of time scales for the translational degrees of freedom and the internal quantum states. An application of the Trotter formula results in the following expression [14, 16, 17] for the partition function $Z_{N_1, V_1, T} = \lim_{P \to \infty} Z_P$ at temperature $T^* = (\beta J)^{-1}$, with

$$\begin{aligned} Z_P(\beta, N_1, V_1) = \frac{A_P^{N_1 P}}{\lambda^{2N_1} N_1!} \int d\mathbf{r}_1 \cdots \int d\mathbf{r}_{N_1} \exp\left[-\beta \sum_{i<j} U(r_{ij}) \right] \\ \times \sum_{\{S\}} \exp\left[-\beta \sum_{i=1}^{N_1} \sum_{p=1}^{P} \left(K_P S_{i,p} S_{i,p+1} \right.\right. \\ \left.\left. + \frac{1}{P} \sum_{i \neq j = 1}^{N_1} J(r_{ij})\, S_{i,p} S_{j,p} \right) \right] \end{aligned} \tag{5}$$

with $A_P = [\frac{1}{2}\sinh(\beta\omega_0/P)]^{1/2}$ and $K_P = (1/2\beta)\ln[\coth(\beta\omega_0/2P)]$, λ is the thermal de Broglie wavelength, the quantum chains have periodic boundary conditions with respect to P, and $S_{i,p} = \pm 1$. N_1 denotes the number of particles in one of the GEMC-boxes at volume V_1. In the GEMC simulation, in addition, all necessary volume and particle decompositions have to be taken into account properly for the full partition function. The Gibbs ensemble simulations [14] were done with $N = 200$ particles and $P/\beta J = 40$. A typical run over 10^6 MC steps (consisting of 200 attempted moves, 20 particle exchange, and 1 volume change attempts) took about 14 CPU h on a CRAY YMP; the same interaction parameters have been chosen as in Ref. 17. In an additional study the phase diagram was analyzed by a combination of PIMC and finite-size scaling techniques [17]. Applying the finite-size block analysis technique [13], sketched above, in conjunction with the density cumulant intersection method [13], the tricritical point at the end of the critical line can be located at $((\beta_{\text{tri}} J)^{-1},\ \rho_{\text{tri}} R^2) = (0.57 \pm 0.02,\ 0.45 \pm 0.01)$. Below the tricritical temperature a paramagnetic (PM) *gas* phase coexists with a ferromagnetic

(FM) *liquid* phase for a certain density window. By cooling the system further down, a sudden jump in the coexistence curve on the high-density side occurs: the system crystallizes into a solid phase. Below this temperature a PM *gas* phase is in coexistence with a *square*-lattice FM *solid* phase. The square lattice is stable, presumably due to the particular choice of the interaction potential $J(r)$ of the square-well type, which favours square lattice structures energetically at low temperatures. The results of the GEMC simulations for the gas–liquid coexistence densities are presented in Table I, together with the NVT-ensemble results of Ref. 17 and MF predictions. Only a weak ensemble dependence of the results can be found. The MF theory predicts a too large coexistence region, resulting in a 100% deviation from the GEMC results for the gas–liquid critical temperature T_c; the latter was found by GEMC to be about $T_c = 0.57$, in good agreement with NVT-ensemble results. The MF study provides a qualitatively correct phase diagram but it underestimates the fluctuations and, in principle, contains only the tricritical exponents of the system in three dimensions. The exponent describing the merging of the phase boundaries in the tricritical point is distinctly smaller than the MF value (unity), resulting in a much flatter shape of the coexistence region, and thus the tricritical temperature is off by a factor of two as compared to PIMC!

Now a modification of the Ramakrishnan–Yussouff theory [19] to the model fluid Eq. (4) is discussed [18]. The magnetic interaction arising from the presence of the internal quantum states is incorporated in the sense of a MF treatment [16] of the attractive interaction in addition to the classical hard-disk contribution to the free energy. The magnetization density $m(\mathbf{r})$ for the ferromagnetic solid is proportional to the number density, i.e., $m(\mathbf{r}) = m_0 \rho(\mathbf{r})$. In the MF model, the magnetic field on one particle due to

Table I. Gas–Liquid Coexistence Densities of the Two-Dimensional Fluid with Internal Quantum States Versus Temperature[a]

	Gibbs–MC		NVT–MC [17]		Mean field	
T^*	ρ_g^*	ρ_l^*	ρ_g^*	ρ_l^*	ρ_g^*	ρ_l^*
0.35	0.139	0.739	0.174	0.711	0.198	0.762
0.4	0.196	0.715	0.232	0.659	0.240	0.744
0.45	0.265	0.685	0.298	0.639	0.276	0.726
0.5	0.323	0.633	0.341	0.576	0.3	0.702
0.55	0.376	0.521	0.399	0.506	0.324	0.684

[a] Comparison of Gibbs ensemble Monte Carlo results with those of an NVT-ensemble simulation and mean field predictions.

the interaction will all other particles is approximated by the average molecular field, $\xi_m(\mathbf{r}) = \int d\mathbf{r}'\, m(\mathbf{r}-\mathbf{r}')\, J(\mathbf{r}')$. The free-energy functional is then given by

$$\beta f([\rho]) = \beta f_{\rm cl}([\rho]) + \frac{\beta}{2}\int \frac{d\mathbf{r}}{V} m(\mathbf{r})\, \xi_m(\mathbf{r}) - \int \frac{d\mathbf{r}}{V} \rho(\mathbf{r}) \ln[2\cosh\{\beta(\xi_m^2(\mathbf{r}) + \omega_0^2/4)^{1/2}\}] \tag{6}$$

$\beta f_{\rm cl}([\rho])$ and the direct correlation function have been taken from the literature [20]. The free-energy functional, Eq. (6), has been minimized with respect to choices of (nonuniform) densities $\rho(\mathbf{r})$ to obtain the Helmholtz free energies of the solid phases [18]. If the Helmholtz free energy in the fluid phase is known from the MF analysis [16], it is straightforward to obtain the $T^* - \rho^*$ phase diagram by performing double-tangent constructions to obtain coexistence densities. For temperatures below $T^* = 5.9$, the system undergoes a second-order transition from a paramagnetic fluid phase at low densities to a ferromagnetic fluid at high densities and a first-order transition from a ferromagnetic fluid to a ferromagnetic hexagonal solid. As expected, the freezing density decreases with decreasing temperature due to the greater stability of the solid phase arising from the magnetic interaction. The DFT predictions for the location of the fluid–solid transition was confirmed by an analysis of the bond-orientation order parameter of MC data [21]. Also, the average magnetization of the solid m_0 is observed to be higher than that of the fluid. At temperatures below the tricritical point $T^*_{\rm TCP}, = 1.25$, one obtains a first-order transition from a paramagnetic gas to a ferromagnetic fluid in addition to the liquid–solid transition. The liquid phase is stable only for temperatures above a first triple temperature $T^*_{\rm TP_1} = 0.55$, while for temperatures below $T^*_{\rm TP_1}$ and above $T^*_{\rm TP_2} = 0.07$, a paramagnetic gas is in coexistence with a ferromagnetic hexagonal solid. The square-lattice solid, observed in the MC simulations [17] at $T^* = 0.16 \pm 0.01$, starts appearing at temperatures below $T^* = 0.09$, and for a range of temperatures $T^*_{\rm TP_2} < T^* < 0.09$ there exists a reentrant transition with the hexagonal solid appearing for low and high densities, separated by a narrow region of square solid stability centered around $\rho^* = 1.0$. Upon lowering temperatures below the paramagnetic gas–ferromagnetic square solid–ferromagnetic hexagonal solid triple point ($T^*_{\rm TP_2}$), a gas phase is in coexistence with a square solid, followed by a square solid–hexagonal solid structural transition at higher densities.

4. RANDOM-FIELD-INDUCED ROUNDING OF THE ISING-TYPE TRANSITION IN PHYSISORBED $(CO)_{1-x}(N_2)_x$ MIXTURES

The statistical thermodynamics of systems with randomly quenched disorder is a real challenge for theory; for an overview see Ref. 22 and references therein. Particularly striking phenomena are predicted in reduced dimensionality, such as the destruction of long-range order of Ising-type systems in $d=2$ dimensions by arbitrarily weak random fields [23]. This absence of true long-range order also shows up in a rounding of the transition even by very weak random fields, which has been confirmed by a recent experiment on $(CO)_{1-x}(N_2)_x$ [24]. Very weak dilution of CO with N_2 molecules (concentrations of 3% or less) produces a strong rounding of the specific heat anomaly of the transition [24]. Assuming that the quadrupole moment and dipole moment of the CO molecules are linearly coupled, one would obtain, from the quadrupole–quadrupole interaction between N_2 and CO, an effective random field acting on the CO dipole moments. For simplicity the system is being described by a simple square lattice, disregarding the actual sublattice structure. If we associate an Ising spin $S_i = \pm 1$ with a CO molecule at site i and $S_i = 0$ with an N_2 molecule at the site, the following Hamiltonian [22] results:

$$H = +\sum_{\langle i,j \rangle} JS_iS_j - \sum_{\langle i,j \rangle} J'S_i(1-S_j^2) \tag{7}$$

Here J is the interaction between the nearest-neighbor pairs of spins (pseudo-dipole–dipole interaction), and J' the hypothetical pseudo-dipole–quadrupole interaction. In this model the sites j taken by N_2 produce a field randomly: sometimes on a site in the sublattice where the spins are up, sometimes in the sublattice where the spins are down. This model is studied by MC methods [22]. Square lattices of sizes $L=24$, 32, 40, 50 are used with periodic boundary conditions and different impurity concentrations x. Averages are taken over 100–200 configurations of the impurity distribution over the lattice for each x. Detailed analysis of the order parameter, susceptibility, and the cumulant [22] are consistent with the interpretation that the transition in the pure system is rounded by the random field.

For the case of pure CO adsorption ($x=0$) the low-temperature ordering of CO physisorbed on graphite has been investigated [25] by MC simulations with finite-size scaling methods, from a realistic microscopic model with continuous orientational degrees of freedom and a recent *ab initio* potential. An analysis of different contributions constituting the total CO–CO interactions reveals that the ordering is not caused by the electrostatic dipole moment, but by the shape asymmetry of the molecule. The ordered ground state may be a ferrielectric herringbone structure with a net dipole moment perpendicular to the herringbone symmetry axis.

ACKNOWLEDGMENTS

Discussions and cooperation with K. Binder, M. O. Ihm, D. Marx, O. Opitz, V. Pereyra, F. Schneider, S. Sengupta, and H. Wiechert and financial support from the Deutsche Forschungsgemeinschaft (Heisenberg Fellowship) are gratefully acknowledged, as well as the granting of computer time on the Cray-YMP (HLRZ Jülich and RHRK Kaiserslautern), VP 100 (RHRK Kaiserslautern), and IBM RISC System/6000 cluster (ZDV Mainz).

REFERENCES

1. S. K. Sinha, *Ordering in Two Dimensions* (North-Holland, Amsterdam, 1980).
2. M. H. W. Chan, A. D. Migone, K. D. Miner, and Z. R. Li, *Phys. Rev. B* **30**:2681 (1984).
3. O. Opitz, D. Marx, S. Sengupta, P. Nielaba, and K. Binder, *Surf. Sci.* **297**:L122 (1993).
4. D. Marx, O. Opitz, P. Nielaba, and K. Binder, *Phys. Rev. Lett.* **70**:2908 (1993); D. Marx, S. Sengupta, and P. Nielaba, *J. Chem. Phys.* **99**:6031 (1993).
5. O. G. Mouritsen and A. J. Berlinsky, *Phys. Rev. Lett.* **48**:181 (1982); O. G. Mouritsen, *Computer Studies of Phase Transitions and Critical Phenomena* (Springer, Berlin, 1984).
6. W. Selke, *Physica A* **177**:460 (1991).
7. F. Y. Wu, *Rev. Mod. Phys.* **54**:235 (1982).
8. V. Privman, P. C. Hohenberg, and A. Aharony, in *Phase Transitions and Critical Phenomena, Vol. 14*, C. Domb and J. L. Lebowitz, eds. (Academic, London, 1991).
9. D. Marx and P. Nielaba, *Phys. Rev. A* **45**:8968 (1992).
10. C. S. Murthy, K. Singer, M. L. Klein, and I. R. McDonald, *Mol. Phys.* **41**:1387 (1980); W. A. Steele, *Surf. Sci.* **36**:317 (1973).
11. T. Biben and J. P. Hansen, *Phys. Rev. Lett.* **66**:2215 (1991).
12. A. Z. Panagiotopoulos, *Mol. Phys.* **61**:813 (1987); *Mol. Simul.* **9**:1 (1992).
13. K. Binder, *Z. Phys.* **B43**:119 (1981); M. Rovere, D. W. Heermann, and K. Binder, *Europhys. Lett.* **6**:585 (1988).
14. F. Schneider, M. O. Ihm, and P. Nielaba, in *Computer Simulation Studies in Condensed Matter Physics VII*, D. P. Landau, K. K. Mon, and H. B. Schüttler, eds. (Springer, Berlin, 1994), p. 188.
15. T. W. Melnyk and B. L. Sawford, *Mol. Phys.* **29**:891 (1975).
16. P. de Smedt, P. Nielaba, J. L. Lebowitz, J. Talbot, and L. Dooms, *Phys. Rev.* **A38**:1381 (1988).
17. D. Marx, P. Nielaba, and K. Binder, *Phys. Rev.* **B47**:7788 (1993).
18. S. Sengupta, D. Marx, and P. Nielaba, *Europhys. Lett.* **20**:383 (1992).
19. T. V. Ramakrishnan and M. Yussouff, *Phys. Rev.* **B19**:2775 (1979); see also A. D. J. Haymet and D. J. Oxtoby, *J. Chem. Phys.* **74**:2559 (1981).
20. C. Ebner, H. R. Krishnamurthy, and R. Pandit, *Phys. Rev.* **A43**:4355, (1990); Y. Rosenfeld, *Phys. Rev.* **A42**:5983 (1990).
21. A. C. Mitus, D. Marx, S. Sengupta, P. Nielaba, A. Z. Patashinskii, and H. Hahn, *J. Phys. Condensed Matter* **5**:8509 (1993).
22. V. Pereyra, P. Nielaba, and K. Binder, *J. Phys. Condensed Matter* **5**:6631 (1993).
23. Y. Imry and S. K. Ma, *Phys. Rev. Lett.* **35**:1399 (1975); K. Binder, *Z. Phys.* **B50**:343 (1983); S. Fishman and A. Aharony, *J. Phys. C Solid State Phys.* **12**:L729 (1979).
24. H. Wiechert and St.-A. Arlt, *Phys. Rev. Lett.* **71**:2090 (1993).
25. D. Marx, S. Sengupta, P. Nielaba, and K. Binder, *Phys. Rev. Lett.* **72**:262 (1994).